Supplemental Material

Monitoring cell type-specific gene expression using ribosomal sequencing *in vivo* during cardiac hemodynamic stress

Shirin Doroudgar[1,2], Christoph Hofmann[1,2], Etienne Boileau[1,2,4], Brandon Malone[1,2,4,*], Eva Riechert[1,2], Agnieszka A. Gorska[1,2], Tobias Jakobi[1,2,4], Clara Sandmann[1,2], Lonny Jürgensen[1,2], Vivien Kmietczyk[1,2], Ellen Malovrh[1,2], Jana Burghaus[1,2], Mandy Rettel[5], Frank Stein[5], Fereshteh Younesi[1,2], Ulrike Anne Friedrich[5], Victoria Mauz[2,3], Johannes Backs[2,3], Günter Kramer[6], Hugo A. Katus[1,2], Christoph Dieterich[1,2,4#], and Mirko Völkers[1,2#]

Correspondence:
Dr. Mirko Völkers
email: mirko.voelkers@med.uni-heidelberg.de

Supplemental Methods

Animal Tissues

All experiments were performed in 9-week-old male mice unless otherwise indicated. The Ribo-tag mice were purchased from Jackson Laboratory (JAX ID 011029). Mice were housed in a temperature- and humidity-controlled facility with a 12-h light-dark cycle. The Ribo-tag mouse was bred to the αMHC-Cre mice and to Cdh5-Cre mice line to obtain *Rpl22*^{HA}-expressing homozygous mice in cardiac myocytes and endothelial cells, respectively. At 9 weeks of age, male mice underwent transverse aortic constriction (TAC; 27 gauge needle) or sham operation, as previously described[1,2]. For echocardiography, mice were anesthetized with 2% isoflurane and scanned using a Vevo2100 imaging system (Visual Sonics, ON, Canada) as previously described[3]. Institutional Animal Care and Use Committee approval was obtained for all animal studies.

Human Tissue:

The characterization of samples and patient data has been approved by the ethics committee, medical faculty of Heidelberg, participants have given written informed consent.
Control tissue from non-failing left ventricular tissue has been obtained commercially (BioCat) or from donor hearts that could not be used for transplantations. For Ribo-seq libraries from DCM patients, explanted tissue during heart transplantation were obtained from the apical part of the free left ventricular wall (LV).

Patient characteristics:

ID	EF (%)	Age	Diagnosis	RNA-seq	Ribo-seq
#1	15	60.3	DCM	Yes	Yes
#2	22	58.6	DCM	Yes	Yes
#3	20	62.7	DCM	Yes	-
#4	18	56	DCM	Yes	-
#5	n.a	47	DCM	-	-
NF1	n.a	50	Non failing	Yes	-
NF2	n.a	61	Non failing	Yes	-
NF3	n.a	23	Non failing	Yes	-
NF 4	n.a	70	Non failing	-	-
NF 5	n.a	62	Non failing	-	-
NF 6	n.a	n.a	Non failing	-	-

Tissues were rinsed with NaCl (0.9%) and immediately transferred and stored in liquid nitrogen. Left ventricular tissue was homogenized using a tissue homogenizer in 5 volumes of ice-cold polysome buffer (20 mM Tris pH 7.4, 10 mM MgCl, 200 mM KCl, 2 mM DTT, 1% Triton X-100, 1U DNAse/µl) containing 100 µg/ml CHX. For complete lysis, the samples were kept on ice for 10 min and subsequently centrifuged at 20,000×g to precipitate cell debris and the supernatant was immediately used in the further steps. From the lysate, 100 µL was used as input, from which RNA was extracted using Trizol. Ribosome footprints were generated after treating the lysate with RNAse I (Ambion). Two libraries were generated according to the mammalian Ribo-seq kit (Illumina). Control RNA from non-failing left ventricular tissue has been obtained commercially (BioCat) or from donor hearts that could not be used for transplantations.

Preparation of Tissue Lysates

For heart homogenates, mice were sacrificed, and their hearts were quickly excised, washed in PBS containing 100 µg/ml cycloheximide (CHX), and snap frozen in liquid nitrogen. Left ventricular tissue was homogenized using a tissue homogenizer in 5 volumes of ice-cold polysome buffer (20 mM Tris pH 7.4, 10 mM MgCl, 200 mM KCl, 2 mM DTT, 1% Triton X-100, 1U DNAse/µl) containing 100 µg/ml CHX. For complete lysis, the samples were kept on ice for 10 min and subsequently centrifuged at 20,000×g to precipitate cell debris and the supernatant was immediately used in the further steps. From the lysate, 100 µL was used as input, from which RNA was extracted using Trizol. The remaining lysate was used for anti-HA IP of polysomes. Anti-HA magnetic beads (Thermo Fisher, 88836; 100µl per heart) were washed with 1000 µL polysome lysis buffer three times. The lysate was then added to anti-HA magnetic beads and incubated with rotation at 4°C overnight. Beads were then washed three times with 500 µL of high salt buffer (20 mM Tris pH 7.4, 10 mM MgCl, 300 mM KCl, 2 mM DTT, 1% Triton X-100). The washed beads were subjected to RNA extraction for library construction or immunoblotting analysis.

Cell Culture

Neonatal rat ventricular myocytes (NRVM) were isolated by enzymatic digestion of 1-4-day-old neonatal rat hearts and purified by Percoll density gradient centrifugation before plating, as described[2]. Cardiac myocytes were cultured at various densities, as described in the figure legends. Tissue culture plates were coated with 5 µg/ml fibronectin in serum free DMEM/F-12 medium for 1h. Briefly, 5×10^5 Percoll-purified cardiac myocytes were plated on 35 mm fibronectin-coated plastic culture wells in DMEM/F-12 medium containing 10% fetal bovine serum. After 24h, the medium was replaced with DMEM/F-12 medium containing 2% fetal bovine serum, and cultures were maintained for 24h before cell lysis.

Preperation of cell lysates and monosomes

NRVMs were lysed in polysome buffer. From the lysate, 100 µL was used as input, from which RNA was extracted using Trizol. The remaining lysate was used for RPF generation using polysome profiles after RNAse1 digestion. For complete lysis, the samples were kept on ice for 10 min and subsequently centrifuged at 20,000×g to precipitate cell debris and the supernatant was immediately used in the further steps. Sucrose solutions were prepared in polysome gradient buffer and 20 U/mL SUPERase-In (Ambion). Sucrose density gradients (10–50% wt/vol) were freshly made in SW40 ultracentrifuge tube using a BioComp Gradient Master (BioComp) according to the manufacturer's instructions. Ribosome footprints were generated after treating the lysate with RNAse I (Ambion). Cell lysates were loaded onto sucrose gradients, followed by centrifugation for 250 min at 220,000×g, 4 °C, in an SW40 rotor. Separated samples were fractionated at 0.375 ml/min by using a fractionation system BioComp Gradient Station (BioComp) that continually monitors OD254 values. Monosomal fractions were collected into tubes at 0.3 mm intervals.

Immunocytofluorescence of Mouse Heart Sections
Hearts were cleared by retroperfusion *in situ* with PBS at 70 mmHg, arrested in diastole with 60 mM KCl, fixed by perfusion for 15 min with 10% formalin (Sigma; HT501128), excised, fixed in formalin for 24 hours at room temperature, and embedded in paraffin. Paraffin-embedded hearts were sectioned and placed on slides, which were then deparaffinized, then rehydrated. Antigen retrieval was achieved by boiling the slides in 10 mM citrate pH 6.0 for 12 min, after which slides were washed several times with distilled water, and once with Tris/NaCl, or TN buffer (100 mM Tris, and 150 mM NaCl). Primary antibodies were diluted in TNB and added to slides which were incubated at 4 °C for approximately 12-16h. Samples were then washed with TN buffer and incubated with secondary antibodies at room temperature in the dark for 2 h. Images were obtained using a Zeiss Observer.Z1 fluorescence microscope. Images were obtained with a 20× objective. Rabbit IgG and a mouse isotype-matching antibody were used as negative controls for anti-HA and anti-Actinin, respectively, to ensure the specificity of the signal. Nuclei were stained with DAPI (D1306, Thermo Fisher Scientific). Of note, no unspecific staining was observed in negative controls with the incubation of primary or secondary antibodies alone.

Adult mouse myocyte isolation
For AMVM isolation, 10-week-old male mice were anesthetized 2days after TAC or Sham surgery with isoflurane, and their hearts were excised. Explanted hearts were retrogradely perfused and digested as described previously[4]. Isolated Cells were lysed in polysome buffer and aliquots were used for subsequent RNA- isolation, protein extraction and quantitative mass-spectometry.

Sample preparation and TMT labeling
Cysteine's were reduced with dithiothreitol at 56°C for 30 minutes (10 mM in 50 mM HEPES, pH 8.5) and further alkylated with 2-chloroacetamide at room temperature, in the dark for another 30 minutes (20 mM in 50 mM HEPES, pH 8.5). Samples were processed using the SP3 protocol[5,6] and on-bead digested with trypsin (sequencing grade, Promega), which was added in an enzyme to protein ratio 1:50 for overnight digestion at 37°C. Peptides were modified with TMT10plex[7] Isobaric Label Reagent (ThermoFisher) according the manufacturer's instructions. For sample clean up, an OASIS® HLB µElution Plate (Waters) was used. Offline high pH reverse phase fractionation was performed out on an Agilent 1200 Infinity high-performance liquid chromatography system, equipped with a Gemini C18 column (3 µm, 110 Å, 100 x 1.0 mm, Phenomenex), resulting in 12 fractions.

Mass spectrometry data acquisition
An UltiMate 3000 RSLC nano LC system (Dionex) equipped with a trapping cartridge (µ-Precolumn C18 PepMap 100, 5µm, 300 µm i.d. x 5 mm, 100 Å) and an analytical column (nanoEase™ M/Z HSS T3 column 75 µm x 250 mm C18, 1.8 µm, 100 Å, Waters). A constant flow of solvent A (0.1% formic acid in water) at 30 µL/min was run onto the trapping column for 6 minutes. Subsequently, peptides were eluted via the analytical column with a constant flow of 0.3 µL/min with increasing percentage of solvent B (0.1% formic acid in acetonitrile) from 2% to 4% in 4 min, from 4% to 8% in 2 min, then 8% to 28% for a further 96 min, and finally from 28% to 40% in another 10 min. The outlet of the analytical column was coupled directly to a QExactive plus (Thermo) mass spectrometer using the proxeon nanoflow source in positive ion mode.The peptides were introduced into the QExactive plus via a Pico-Tip Emitter 360 µm OD x 20 µm ID; 10 µm tip (New Objective) and an applied spray voltage of 2.3 kV. The capillary temperature was set at 320°C. Full mass scan was acquired with mass range 350-1400 m/z in profile mode in the FT with resolution of 70000. The filling time was set at maximum of 100 ms with a limitation of $3x10^6$ ions. Data dependent acquisition (DDA) was performed with the resolution of the Orbitrap

set to 35000, with a fill time of 120 ms and a limitation of $2x10^5$ ions. A normalized collision energy of 32 was applied. A loop count of 10 with count 1 was used and a minimum AGC trigger of $2e^2$ was set. Dynamic exclusion time of 30 s was used. The peptide match algorithm was set to 'preferred' and charge exclusion 'unassigned', charge states 1, 5 - 8 were excluded. MS^2 data was acquired in profile mode[8].

MS data analysis
IsobarQuant[9] and Mascot (v2.2.07) were chosen for data processing. A Uniprot *Mus musculus* (UP000000589) proteome database containing common contaminants and reversed sequences was used. The search parameters were the following: Carbamidomethyl (C) and TMT10 (K) (fixed modification), Acetyl (N-term), Oxidation (M) and TMT10 (N-term) (variable modifications). A mass error tolerance of 10 ppm was set for the full scan (MS1) and for MS/MS (MS2) spectra of 0.02 Da. Trypsin was selected as protease with an allowance of maximum two missed cleavages. A minimum peptide length of seven amino acids and at least two unique peptides were required for a protein identification. The false discovery rate on peptide and protein level was set to 0.01.

Data analysis
The protein.txt output file of IsobarQuant were used for the downstream data analysis using the R programming language (ISBN 3-900051-07-0). As a quality filter, only proteins that were quantified with at least two unique peptides were used for the analysis (2527 proteins). The 'signal_sum' columns were first batchcleaned using the 'removeBatchEffect' function from the limma package[10] and further normalized using the vsn package[11]. Limma was employed again to test for differential expression. The resulting fold changes were correlated with changes in Ribo-seq and RNA-seq.

Immunoblotting
Samples were combined with the appropriately concentrated form of Laemmli sample buffer and then boiled before SDS-PAGE followed by transfer to PVDF membranes. The membranes were probed with the following antibodies: HA (Covance, MMS101P; 1:20000), RPL22 (LSBIO, C354480; 1:1000), Eef2 (Cell Signaling, 2332; 1:15000), Pdk4 (Abcam, Ab214938; 1:15000), 4Ebp1 (Cell Signaling, 9644; 1:15000), Csq (Thermo-Fisher, PA1-91; 1:10000), FNIP1 (Proteintech, 19847-1-AP, 1000), FLCN (Cell Signaling, 3697, 1:1000), Desmin (Thermo Fisher, MA5-13259, 1:20000).

Quantitative Real-time PCR
Total RNA was isolated from frozen heart or cultured cells by using Quick-RNA™ MiniPrep (Zymo Research) and reverse-transcribed into complementary DNA (cDNA) by using High Capacity cDNA Reverse Transcription Kit (Applied Biosystems). Quantitative real-time PCR was performed on all samples in triplicate using iTAQ™ SYBR Green PCR Kit (Biorad) according to the manufacturer's instructions.

Parallel Generation of Ribo-seq and RNA-seq Libraries
For each animal, the heart was lysed in 700 µl lysis buffer (20 mM Tris pH 7.4, 10 mM MgCl, 200 mM KCl, 2 mM DTT, 100 ug/ml CHX, 1%Triton X-100,1U DNAse/ul) using a tissue homogenizer (Bullet Blender, NextAdvance). The tissue was homogenized further by passing the lysate through a 23-gauge syringe needle ten times. Homogenates were centrifuged at 4°C and 18,000×g for 10 min, and the supernatant was immediately used in the further steps. For complete lysis, the samples were kept on ice for 10 min and subsequently centrifuged at 20,000×g to precipitate cell debris.
To accurately dissect translation and transcription, both Ribo-seq and RNA-seq libraries were prepared for each biological replicate from the identical lysate. Ribosome footprints were

generated after immunoprecipitation of cardiac myocyte-specific polysomes with Anti-HA magnetic beads after treating the lysate with RNAse I (Ambion). Libraries were generated according the to the mammalian Ribo-seq kit (Illumina). Barcodes were used to perform multiplex sequencing and create sequencing pools containing at least eight different samples and always an equal amount of both RNA and RPF libraries. Sample pools were sequenced on the HiSeq 2000 platform using 50-bp sequencing chemistry.

Human Heart Ribo-seq libraries

Human tissues from explanted human hearts from patients suffering chronic heart failure have been used for RNA-seq and Ribo-seq to confirm conservation of identified sORFs across species. Libraries have been generated according the to the mammalian Ribo-seq kit (Illumina)

Sequencing Data Processing and Quality Control

Adapters removal was done with Flexbar v3.0.3[12] using standard filtering parameters (no prior trimming). Reads with more than 1 uncalled base were not included in the output: *flexbar --max-uncalled 1 --pre-trim-left 0.* Reads aligning to a custom bowtie2 v2.3.0[13] ribosomal index were discarded. Remaining reads were then aligned in genome and transcriptome coordinates with a splice-aware aligner (STAR, v2.5.3a[14], inserting annotations on the fly: *STAR --quantMode TranscriptomeSAM --alignIntronMin 20 --alignIntronMax 100000 --outFilterMismatchNmax 1 --outFilterIntronMotifs RemoveNoncanonicalUnannotated --outFilterMismatchNoverLmax 0.04 --sjdbOverhang 50.* We used the EnsEMBL mouse genome assembly GRCm38.p6, where all non-coding regions were excluded, and all fully contained shorter CDSs were collapsed: *gffread -C -M -K*[15].

Reads mapping anti-sense were discarded based on library strandedness (second-strand for Ribo-seq, first-strand for RNA-seq). Finally, only reads mapping uniquely to only one genomic position as well as to the transcriptome were kept for analysis. For Ribo-seq data, only periodic fragment lengths were kept that showed a distinctive triplet periodicity. We used the automatic Bayesian selection of read lengths and ribosome P-site offsets (BPPS) method[16] to select and shift aligned reads to properly account for the P-site of the ribosome. For the RNA-seq data, reads were trimmed from the 3' end after adapter removal, such that the read length before alignment did match the maximum periodic fragment length of the corresponding Ribo-seq sample, as determined with the BPPS method. Finally, abundance estimates and read count information for the mapped and filtered data were obtained using Stringtie[17] in reference only mode: *stringtie -e -G --rf/--fr.*

For the statistical analyses, we follow the protocol as outlined in Schäfer et al.[18] Briefly, we pinpoint translational control by identifying significantly differential read counts in Ribo-seq and RNA-seq data across conditions and categorize differential gene expression events specific to either both or only one data set type. We use the edgeR package[19] with a four-factor design matrix (RNA-seq cond1, RNA-seq cond2, Ribo-seq cond1 and Ribo-seq cond2) to accomplish this task. We only consider data points with read count observations across all replicates. We used an FDR<0.05 and FC=2 ($\log_2$ FC=1) as cutoff.

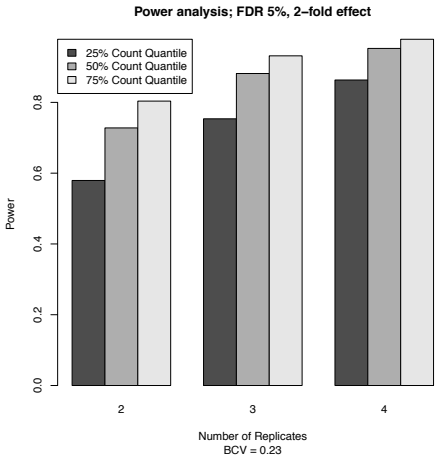

A power analysis was performed in R using the Bioconductor package RNASeqPower As a typical example from our Ribo-Seq setup, we selected the TAC 2d timepoint. We estimated the biological coefficient of

variation (BCV) using the edgeR package and used this information in the rnapower function to estimate power for effect sizes of 2- fold (log_2 FC=1) in Ribo-seq count abundance. For simplicity, we modelled a balanced design of 2 groups with either 2,3, or 4 replicates each. The false discovery rate cutoff was set to a typical value of 5% and three representative gene loci were modelled (low, medium, and high expression). The results are presented in the figure and can be summarized as follows: Our ability (power) to detect a 2-fold expression change with 2 replicates ranges from 0.5 to 0.8 and with 4 replicates from 0.8 to 0.9.

Gene Ontology Analysis
GO term enrichment analysis and KEGG pathway analysis was performed using significantly altered genes as described in each corresponding figure. For biological process analysis, GOTERM_BP_DIRECT in DAVID v6.8 was used with the subset of expressed protein-coding genes as background set. Only enriched GO terms with at least three significantly changed genes were kept for further analysis and ranked by Fisher Exact. Top enriched terms were retained and visualized with a custom plotting routine showing enrichment p-value.

Clustering Analysis
CPMs of significantly changed transcripts of FDR < 0.05 that are expressed in all samples were considered for analysis. Hierarchical clustering analysis was performed with the R package 'pheatmap' using 'ward.D2' and 'euclidean' distance algorithm. For functional analysis of transcript clusters, individual transcripts in each analyzed cluster were extracted and used for Gene Ontology analysis.

miRNA-Motif Enrichment and PhastCon analyis:
TargetScan was used with the R-package to predict biological targets of miRNAs by searching for a presence of conserved 8mer and 7mer sites in translational regulated transcripts that match the seed region of each miRNA. We used the phastCons scores for multiple alignments from the Euarchontoglire subset to the mouse genome, downloaded from the UCSC Genome Browser. The scores were mapped to both translated uORFs and the canonical coding sequences (CDS) that were predicted by Rp-Bp, and to the upstream untranslated regions flanking the uORFs. To define the flanking regions of the uORFs, we extended each uORF exons by 1000 nucleotides upstream, ensuring that the resulting untranslated exons did not overlap with any of the uORF exons. Each regions (uORF, CDS and untranslated flanking regions) were split into 100 nucleotides window over which phastCons scores were average for representation.

Supplemental Tables and Data

Online Table I:
Gene ontology analysis of genes with high ribosomal density in aMHC Cre Ribo-tag mice

Online Table II
Numbers of uORFs in mouse, rat and human samples

Online Table II:
Enriched miRNA motifs in translational regulated genes

Online Table IV:
Ribo-Seq QC Data: Number of reads filtered at each step in the pipeline for Ribo-seq.
Periodicity: Aligned read length distribution before periodicity estimation for Ribo-seq and Periodic lengths and offsets obtained with the BPPS method, for Ribo-seq.

Supplemental References:

1. Rockman HA, Ross RS, Harris AN, Knowlton KU, Steinhelpert ME, Fieldt LJ, Ross J, Chien KR, Steinhelper ME, Field LJ. Segregation of atrial-specific and inducible expression of an atrial natriuretic factor transgene in an in vivo murine model of cardiac hypertrophy. *Proc Natl Acad Sci U S A* [Internet]. 1991;88:8277–81. Available from: http://www.pubmedcentral.nih.gov/articlerender.fcgi?artid=52490&tool=pmcentrez&rendertype=abstract
2. Doroudgar S, Völkers M, Thuerauf DJ, Khan M, Mohsin S, Respress JL, Wang W, Gude N, Müller OJ, Wehrens XHT, Sussman MA, Glembotski CC. Hrd1 and ER-associated protein degradation, ERAD, are critical elements of the adaptive ER stress response in cardiac myocytes. *Circ Res*. 2015;117:536–546.
3. Tsujita Y, Kato T, Sussman MA. Evaluation of left ventricular function in cardiomyopathic mice by tissue Doppler and color M-mode Doppler echocardiography. *Echocardiography*. 2005;22:245–253.
4. Lehmann LH, Jebessa ZH, Kreusser MM, Horsch A, He T, Kronlage M, Dewenter M, Sramek V, Oehl U, Krebs-Haupenthal J, von der Lieth AH, Schmidt A, Sun Q, Ritterhoff J, Finke D, Völkers M, Jungmann A, Sauer SW, Thiel C, Nickel A, Kohlhaas M, Schäfer M, Sticht C, Maack C, Gretz N, Wagner M, El-Armouche A, Maier LS, Londoño JEC, Meder B, Freichel M, Gröne H-J, Most P, Müller OJ, Herzig S, Furlong EEM, Katus HA, Backs J. A proteolytic fragment of histone deacetylase 4 protects the heart from failure by regulating the hexosamine biosynthetic pathway. *Nat Med* [Internet]. 2018 [cited 2019 Jun 4];24:62–72. Available from: http://www.ncbi.nlm.nih.gov/pubmed/29227474
5. Hughes CS, Foehr S, Garfield DA, Furlong EE, Steinmetz LM, Krijgsveld J. Ultrasensitive proteome analysis using paramagnetic bead technology. *Mol Syst Biol* [Internet]. 2014 [cited 2019 Jun 7];10:757. Available from: http://www.ncbi.nlm.nih.gov/pubmed/25358341
6. Hughes CS, Moggridge S, Müller T, Sorensen PH, Morin GB, Krijgsveld J. Single-pot, solid-phase-enhanced sample preparation for proteomics experiments. *Nat Protoc* [Internet]. 2019 [cited 2019 Jun 7];14:68–85. Available from: http://www.nature.com/articles/s41596-018-0082-x
7. Werner T, Sweetman G, Savitski MF, Mathieson T, Bantscheff M, Savitski MM. Ion Coalescence of Neutron Encoded TMT 10-Plex Reporter Ions. *Anal Chem* [Internet]. 2014 [cited 2019 Jun 7];86:3594–3601. Available from: http://pubs.acs.org/doi/10.1021/ac500140s
8. Strucko T, Zirngibl K, Pereira F, Kafkia E, Mohamed ET, Rettel M, Stein F, Feist AM, Jouhten P, Patil KR, Forster J. Laboratory evolution reveals regulatory and metabolic trade-offs of glycerol utilization in Saccharomyces cerevisiae. *Metab Eng* [Internet]. 2018 [cited 2019 Jun 7];47:73–82. Available from: https://www.sciencedirect.com/science/article/pii/S1096717617304032
9. Franken H, Mathieson T, Childs D, Sweetman GMA, Werner T, Tögel I, Doce C, Gade S, Bantscheff M, Drewes G, Reinhard FBM, Huber W, Savitski MM. Thermal proteome profiling for unbiased identification of direct and indirect drug targets using multiplexed quantitative mass spectrometry. *Nat Protoc* [Internet]. 2015 [cited 2019 Jun 7];10:1567–1593. Available from: http://www.ncbi.nlm.nih.gov/pubmed/26379230
10. Ritchie ME, Phipson B, Wu D, Hu Y, Law CW, Shi W, Smyth GK. limma powers differential expression analyses for RNA-sequencing and microarray studies. *Nucleic Acids Res* [Internet]. 2015 [cited 2019 Jun 7];43:e47–e47. Available from: http://www.ncbi.nlm.nih.gov/pubmed/25605792
11. Huber W, von Heydebreck A, Sultmann H, Poustka A, Vingron M. Variance stabilization applied to microarray data calibration and to the quantification of differential expression.

Bioinformatics [Internet]. 2002 [cited 2019 Jun 7];18:S96–S104. Available from: https://academic.oup.com/bioinformatics/article-lookup/doi/10.1093/bioinformatics/18.suppl_1.S96
12. Dodt M, Roehr J, Ahmed R, Dieterich C. FLEXBAR—Flexible Barcode and Adapter Processing for Next-Generation Sequencing Platforms. *Biology (Basel)* [Internet]. 2012;1:895–905. Available from: http://www.mdpi.com/2079-7737/1/3/895/
13. Langmead B, Salzberg SL. Fast gapped-read alignment with Bowtie 2. *Nat Methods* [Internet]. 2012;9:357–9. Available from: http://www.ncbi.nlm.nih.gov/pubmed/22388286%0Ahttp://www.pubmedcentral.nih.gov/articlerender.fcgi?artid=PMC3322381
14. Dobin A, Davis CA, Schlesinger F, Drenkow J, Zaleski C, Jha S, Batut P, Chaisson M, Gingeras TR. STAR: ultrafast universal RNA-seq aligner - Supplementary Data. *Bioinformatics* [Internet]. 2013;29:15–21. Available from: http://bioinformatics.oxfordjournals.org/content/suppl/2012/10/25/bts635.DC1/Dobin.STAR.Supplementary.Response2.pdf
15. Baren J Van, Salzberg SL, Wold BJ, Pachter L, Trapnell C, Williams BA, Pertea G, Mortazavi A, Kwan G, van Baren MJ. Transcript assembly and quantification by RNA-Seq reveals unannotated transcripts and isoform switching during cell differentiation. *Nat Biotechnol* [Internet]. 2010;28:511–515. Available from: https://www.scienceopen.com/document_file/ea7391c3-e986-4bad-b7e1-740baee6d961/PubMedCentral/ea7391c3-e986-4bad-b7e1-740baee6d961.pdf
16. Malone B, Atanassov I, Aeschimann F, Li X, Großhans H, Dieterich C. Bayesian prediction of RNA translation from ribosome profiling. *Nucleic Acids Res*. 2016;45:2960–2972.
17. Pertea M, Kim D, Pertea GM, Leek JT, Salzberg SL. Transcript-level expression analysis of RNA-seq experiments with HISAT, StringTie and Ballgown. *Nat Protoc*. 2016;11:1650–1667.
18. Schafer S, Adami E, Heinig M, Rodrigues KEC, Kreuchwig F, Silhavy J, Van Heesch S, Simaite D, Rajewsky N, Cuppen E, Pravenec M, Vingron M, Cook SA, Hubner N. Translational regulation shapes the molecular landscape of complex disease phenotypes. *Nat Commun*. 2015;6:7200.
19. McCarthy DJ, Chen Y, Smyth GK. Differential expression analysis of multifactor RNA-Seq experiments with respect to biological variation. *Nucleic Acids Res*. 2012;40:4288–4297.

Online Figures

Online Figure I

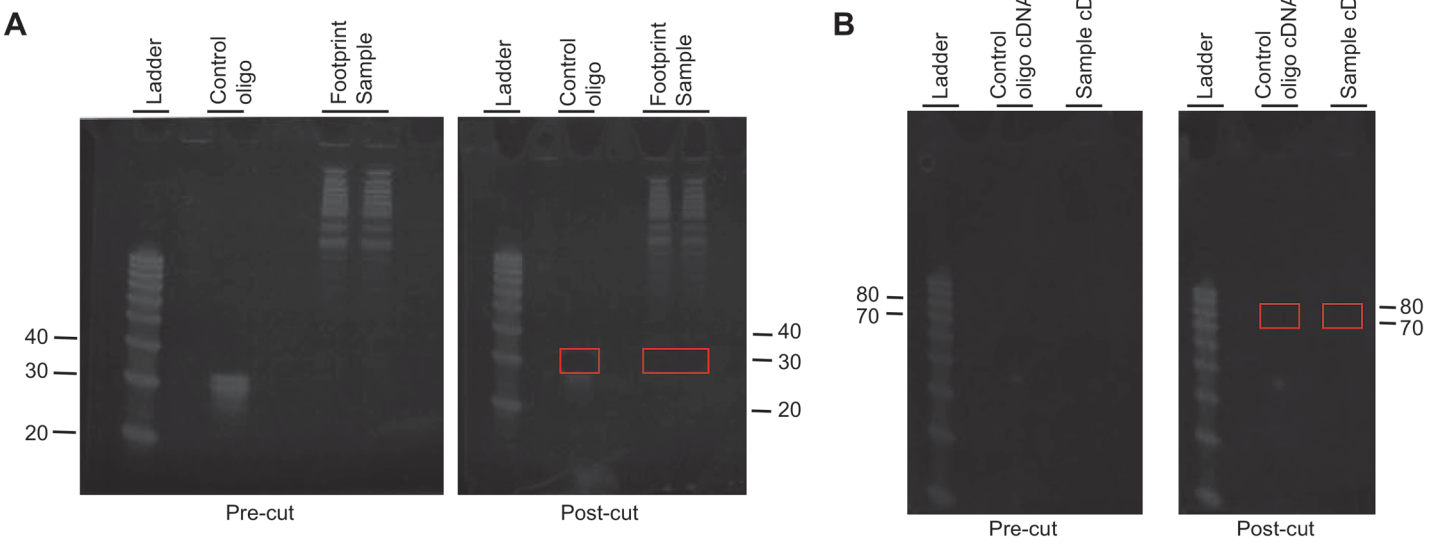

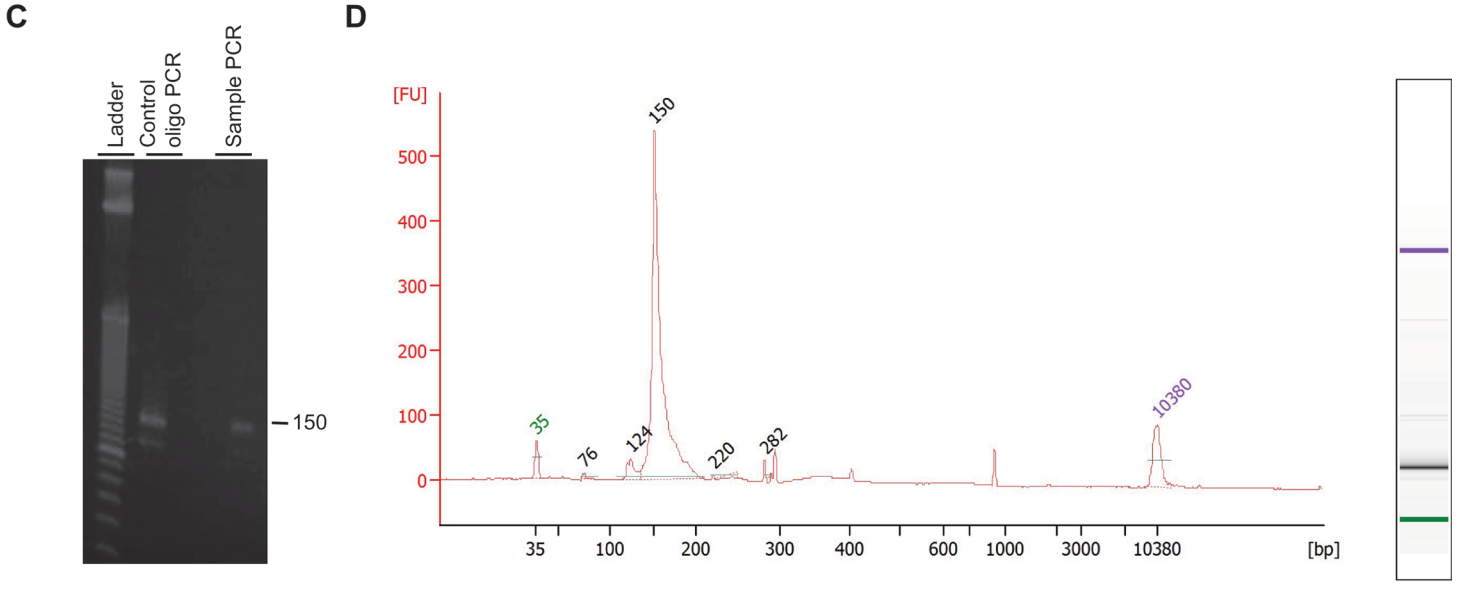

Overall Results for sample 3 : N2-6

Number of peaks found: 5 Noise: 0,4

Peak table for sample 3 : N2-6

Peak	Size [bp]	Conc. [pg/µl]	Molarity [pmol/l]	Observations
1	35	125,00	5.411,3	Lower Marker
2	76	20,85	417,3	
3	124	108,60	1.329,2	
4	150	1.878,34	18.914,5	
5	220	3,65	25,2	
6	282	12,55	67,5	
7	10.380	75,00	10,9	Upper Marker

Online Figure I. Preparation of a Ribo-seq Library

A, Size selection of footprint fragments. Isolated footprint fragments were loaded on a 15% (wt/vol) TBE-urea polyacrylamide gel. The gel was stained with SYBR Gold (pre-cut) and the region of interest (marked with the red box) was excised (post-cut). A phosphorylated RNA control oligonucleotide was included as an internal control of the method. **B,** Reverse-transcribed products are separated from the non-ligated linker by denaturing PAGE, and the single-stranded DNA is excised from the gel. **C,** Quality control gel of PCR which is performed to amplify the circularized, single-stranded DNA and to introduce a bar code using Phusion polymerase. **D,** PCR products are purified using AMPure XP beads and quantified with a Bioanalyzer high-sensitivity DNA chip, before being sequenced with sequencing and bar-coding primers.

Online Figure II

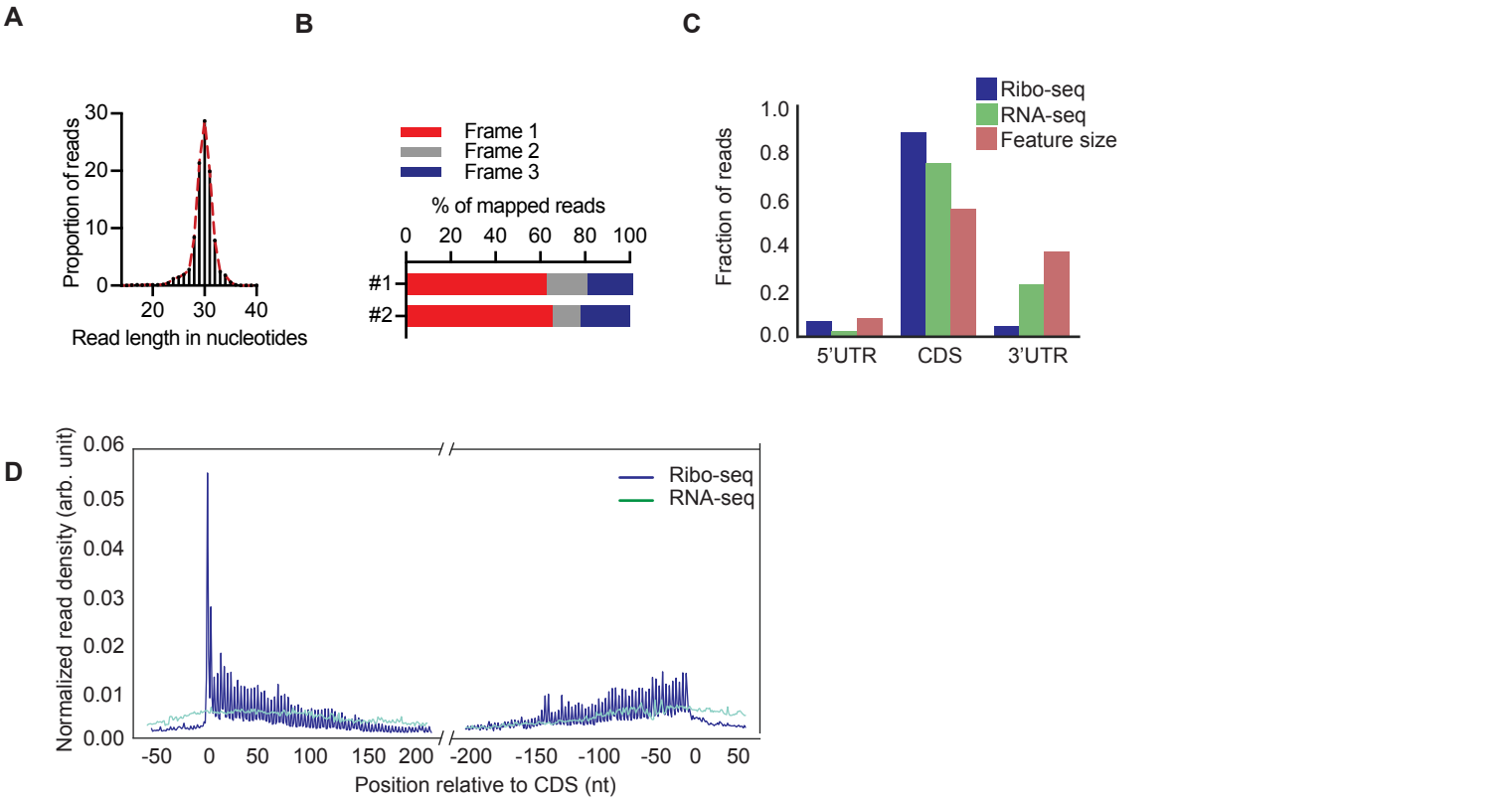

Online Figure II. Quality Control of Ribo-seq Libraries
A, Read length distribution of ribosome-protected fragment (RPF). **B,** bar plot summarizes RPF periodicity as the percentage of footprints that match primary reading frames of annotated CDS genome-wide. **C,** Fraction of reads in different gene regions from Ribo-seq and RNA-seq. Included are reads uniquely mapped in CDS and UTR regions. **D,** Metagene analysis built around annotated translation initiation and termination sites for Ribo-seq and RNA-seq. The raw counts at each position are normalized by the total counts across the window size for each sample. The metagene average is calculated by taking the median of normalized counts at each position. For Ribo-seq, periodic fragments were considered for the analysis and shifted according to their P-site offsets. For RNA-seq, all fragment lengths were considered, up to the maximum periodic fragment length of the corresponding Ribo-seq sample; however, to be included in the metagene average, a minimum count was required in the normalization window.

Online Figure III

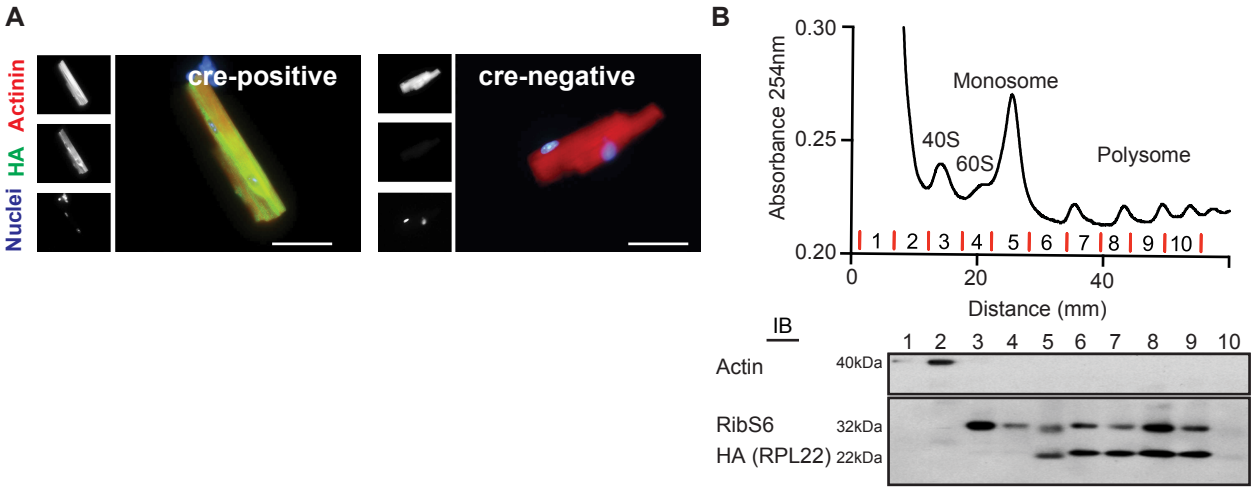

Online Figure III. Immunocytofluorescence and Immunoblot Characterization of Ribo-tag Mice.
A, Immunocytofluorescent confocal images of isolated cardiac myocytes from cre-positive and cre-negative αMHC-Cre:Ribo-tag ventricles. Bar graph 25μm. **B,** Upper panel: Polysome profile of an αMHC-Cre:Ribo-tag mouse left ventricle, absorbance of light at 254 nm. Lower panel: Immunoblot of trichloroacetic acid-precipitated polysomal fractions confirming HA incorporation into actively translating ribosomes.

Online Figure IV

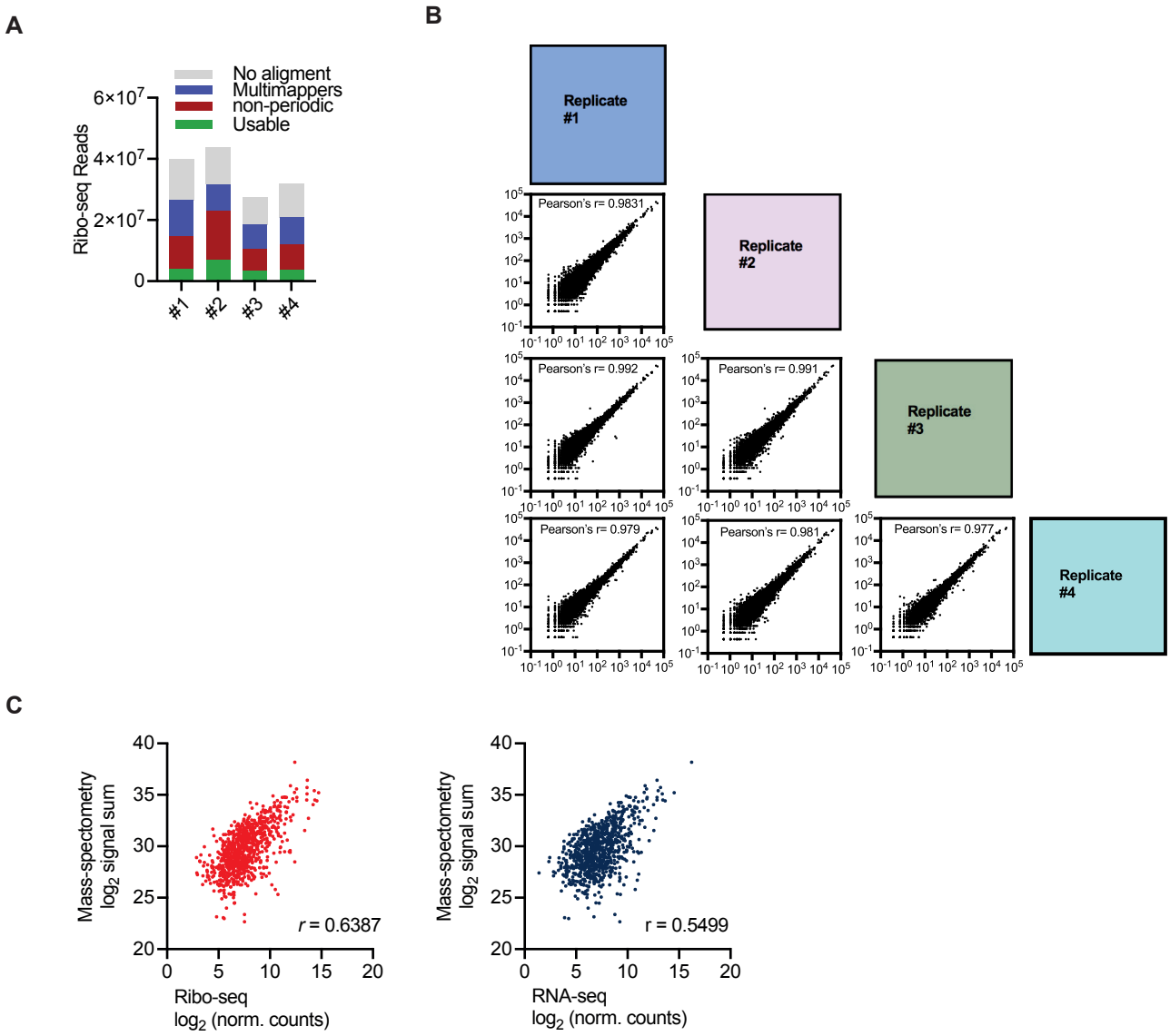

Online Figure IV. Ribo-seq of Cardiac Myocytes *in vivo*
A, Ribo-seq read counts of four different libraries showing periodic (usable), non-periodic, and multi-mapped reads, when mapped to the mouse transcriptome. **B,** Scatter plots for pairwise comparisons of the $\log_2$ fold change of counts per million mapped reads (CPM) for annotated transcripts in four different Ribo-seq libraries. Pearson correlation coefficient r between different libraries > 0.97.
C, Gene-based scatterplot showing the correlation between mean Ribo-seq (red) or RNA-seq expression levels (blue) and protein abundance derived from isolated myocytes. Correlation coefficients are Pearson's r values.

Online Figure V

A

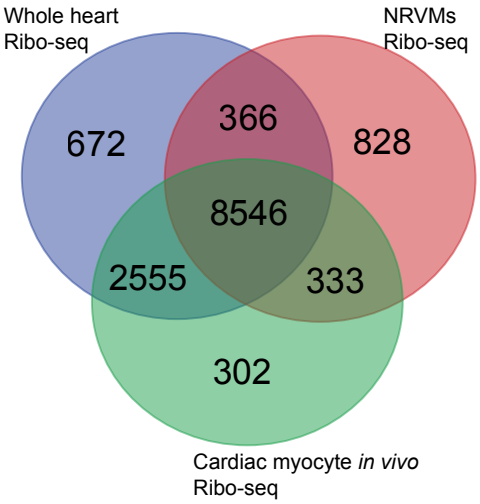

B

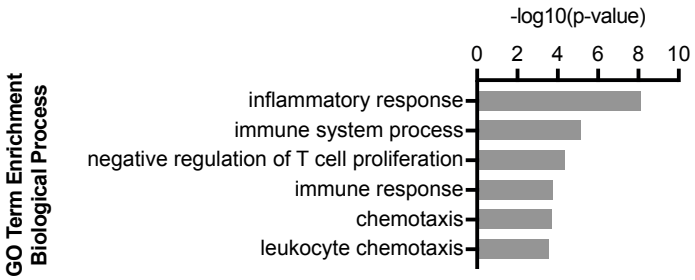

Online Figure V. Mouse Translatome
A, Venn diagram showing the overlap between the cardiac myocyte translatome (*in vitro*), the whole heart translatome (*in vivo*) and myocyte specific Ribo-tag translatome. **B,** Enrichment of significant non myocytes GO terms in the whole heart only group (672 transcripts). Fisher's exact test.

Online Figure VI

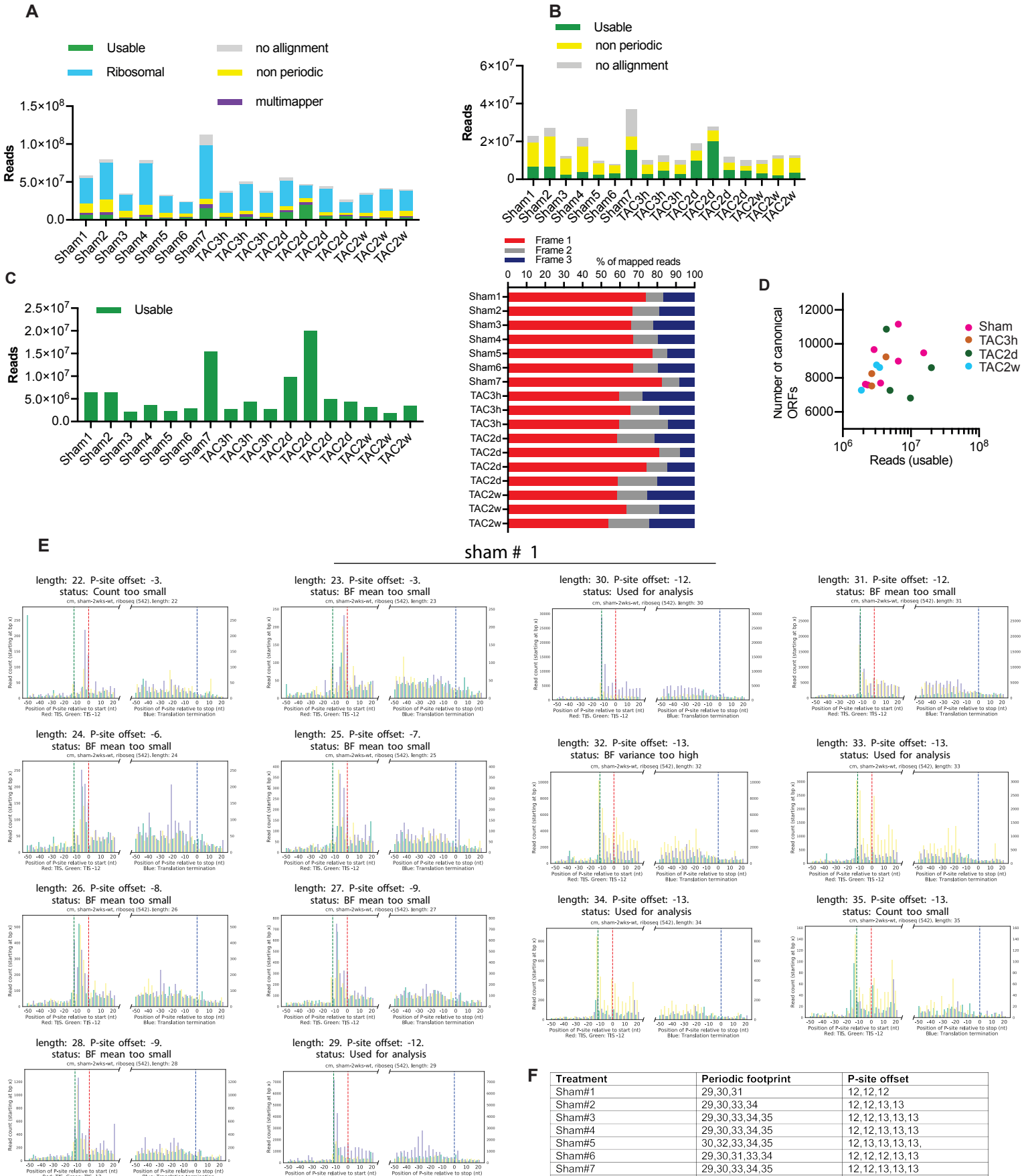

F

Treatment	Periodic footprint	P-site offset
Sham#1	29,30,31	12,12,12
Sham#2	29,30,33,34	12,12,13,13
Sham#3	29,30,33,34,35	12,12,13,13,13
Sham#4	29,30,33,34,35	12,12,13,13,13
Sham#5	30,32,33,34,35	12,13,13,13,13,
Sham#6	29,30,31,33,34	12,12,12,13,13
Sham#7	29,30,33,34,35	12,12,13,13,13
TAC 3h #1	29,30,31,32,32,33	12,12,12,13,13,13
TAC 3h #2	30,31,33,34,35	12,12,13,13,13,
TAC 3h #3	29,30,33,34,35	12,12,13,13,13
TAC 2d #1	29,30,32,33,	12,12,12,12
TAC 2d #2	32,33,34,35	12,12,12,13
TAC 2d #3	32,33,34,35	10,10,13,13
TAC 2d #4	29,30,32	12,12,13
TAC 2w #1	29,30,33,33,34,35	12,12,13,13,13,13
TAC 2w #2	29,30,32,33,34,35	12,12,13,13,13,13
TAC 2w #3	29,29,39,32,33,34,35	9,12,12,13,13,13,13

Online Figure VI. Ribo-seq of Stressed Mouse Myocardium

A-C Ribo-seq read counts of all used libraries showing periodic (usable), non-periodic, and multi-mapped reads, when mapped to the mouse transcriptome. Bar plot summarizes RPF periodicity for all used samples as the percentage of footprints that match primary reading frames of annotated CDS genome-wide. **D,** Scatter plot of usable reads vs detected ORFs in indicated experimental models. **E,** Graphical representation of the periodic profile Bayesian model selection showing results for different read lengths and p-site offsets for one typical library. **F,** Periodic footprint lengths and P-offset for all used libraries. BF = Bayes Factor. For details, see Malone, B., Atanassov, I., Aeschimann, F., Li, X.,Großhans, H., Dieterich, C.: Nucleic Acids Research 45(6), 2960–2972 (2017).

Online Figure VII

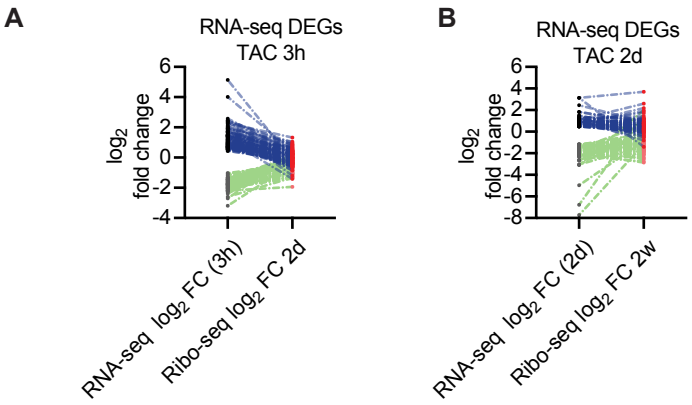

Online Figure VII. Differentially regulated genes at different timepoints. log_2 FC of RNA-seq of DEGs at 3h after TAC followed on the Ribo-seq level 2d after TAC (**A**) and Log_2 FC of RNA-seq of DEGs at 2d after TAC followed on the Ribo-seq level 2w after TAC (**B**). Blue lines indicate significantly upregulated DEGs at the RNA-seq level at 3h or 2d after TAC. Green lines indicate significantly downregulated DEGs at the RNA-seq level at 3h or 2d after TAC.

Online Figure VIII

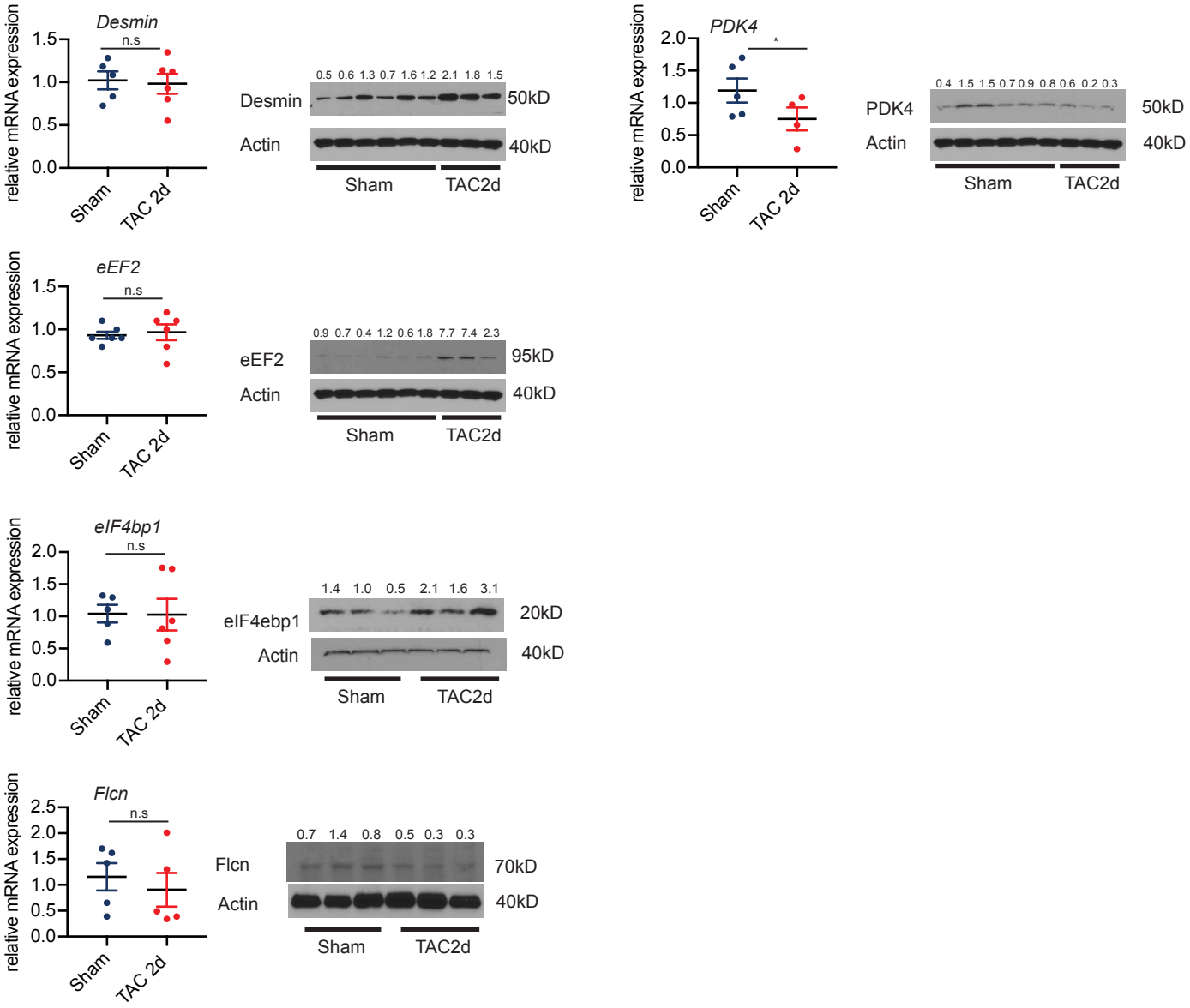

Online Figure VIII. Immunoblot validation.
Validation of selected regulated transcripts by immunblots and RT-PCR analysis .
by immunblots and RT-PCR analysis. *p>0.05 (t-test).Quantification of fold-changes in protein levels are shown on top of the immunoblots normalized to Sham operated animals. For some cases the same membrane was used to detect several proteins and therefore share the same loading control.

Online Figure IX

A

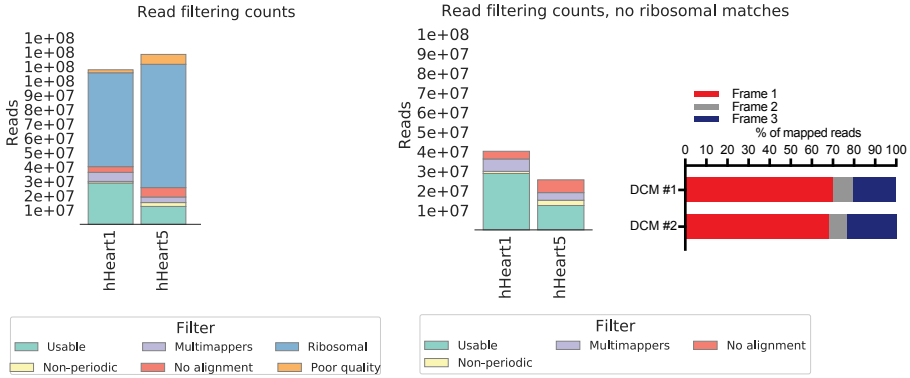

B

hHeart1

Length: 19. P-site offset: -2. Status: Count too small

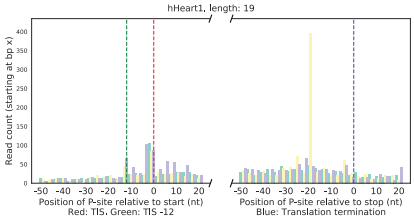

Length: 20. P-site offset: -3. Status: BF mean too small

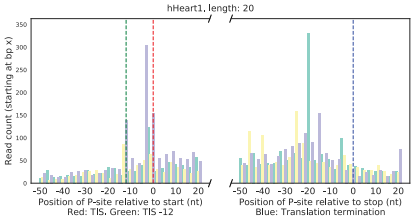

Length: 21. P-site offset: -3. Status: Used for analysis

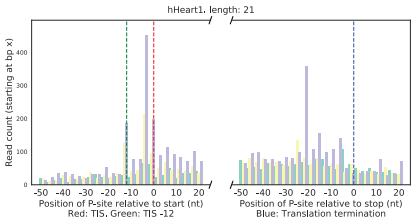

Length: 22. P-site offset: -3. Status: BF mean too small

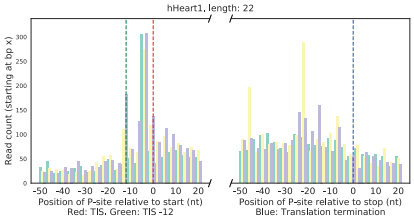

Length: 23. P-site offset: -6. Status: Used for analysis

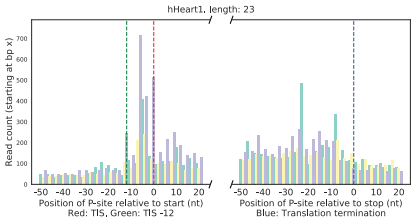

Length: 24. P-site offset: -7. Status: BF mean too small

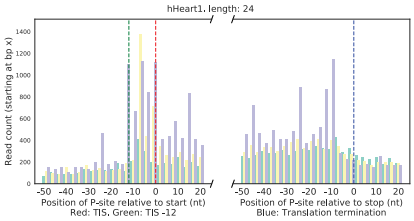

Length: 25. P-site offset: -8. Status: BF mean too small

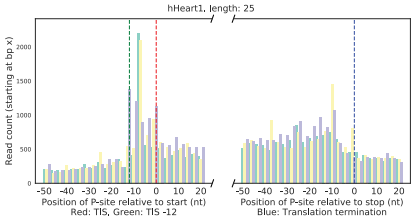

Length: 26. P-site offset: -9. Status: Used for analysis

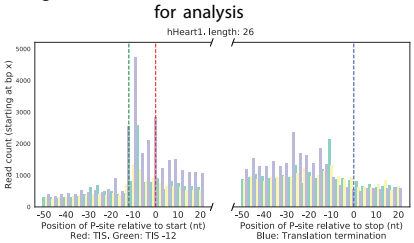

Length: 27. P-site offset: 0. Status: Used for analysis

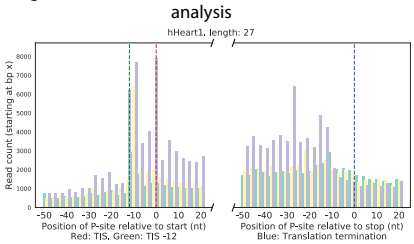

Length: 28. P-site offset: -12. Status: Used for analysis

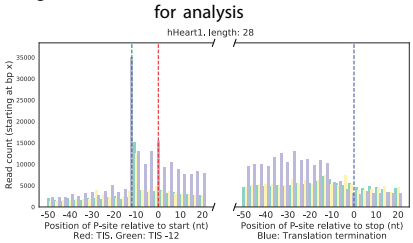

Length: 29. P-site offset: -12. Status: Used for analysis

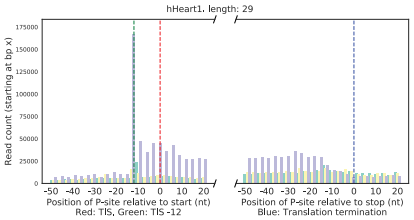

Length: 30. P-site offset: -12. Status: Used for analysis

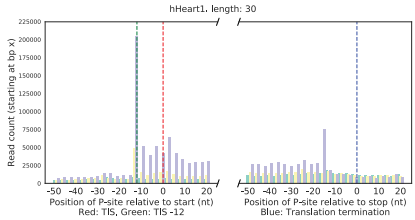

Length: 31. P-site offset: -12. Status: Used for analysis

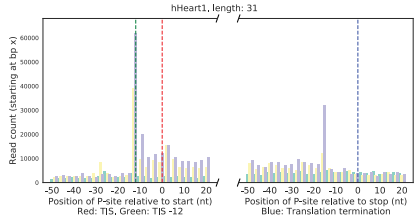

Length: 32. P-site offset: -13. Status: Used for analysis

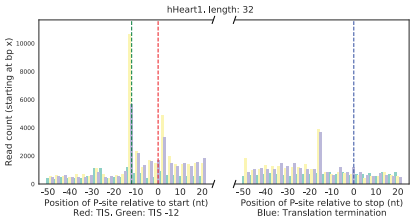

Length: 34. P-site offset: -12. Status: BF mean too small

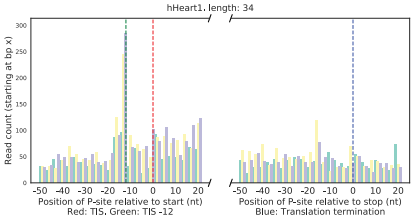

Length: 33. P-site offset: -13. Status: BF mean too small

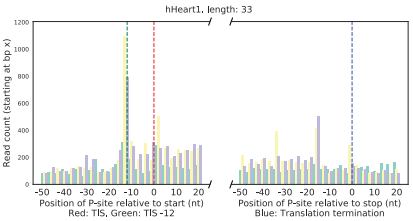

Length: 35. P-site offset: -12. Status: Count too small

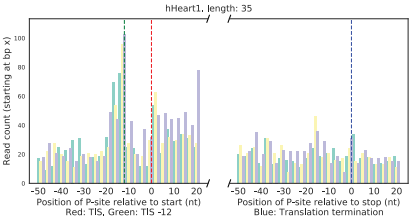

Online Figure IX. Ribo-seq of Human Myocardium

A, Ribo-seq read counts of two different libraries showing periodic (usable), non-periodic, and multi-mapped, reads when mapped to the human transcriptome. Bar plot summarizes RPF periodicity for all used samples as the percentage of footprints that match primary reading frames of annotated CDS genome-wide.

B, Graphical representation of the periodic profile Bayesian model selection showing results for different read lengths and p-site offsets.

Online Figure X

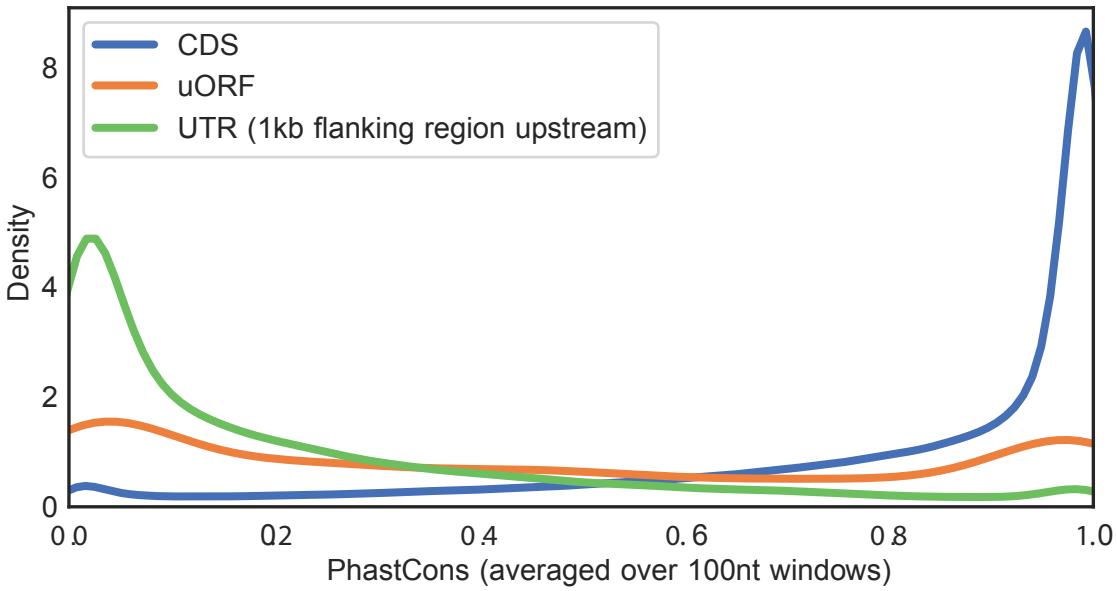

Online Figure X. Conservation Analysis of uORFs
Conservation levels of uORF, 5'UTR and protein-coding CDS computed using phastCons.